OPEN ACCESS



JWST's TEMPLATES for Star Formation: The First Resolved Gas-phase Metallicity Maps of Dust-obscured Star-forming Galaxies at z ~ 4

Jack E.Birkin ¹, Taylor A. Hutchison ²⁵, Brian Welch ³⁴, Justin S.Spilker ¹, Manuel Araven ⁵, Matthew B. Bayliss ⁶, Jared Cather ⁵, Scott C.Chapma ^{8,9,10}, Anthony H. Gonzale ⁷, Gayathri Gururaja ^{1,12}, Christopher C.Hayward ³, Gourav Khulla ¹, Keunho J.Kim ⁶, Guillaume Mahle ^{1,5,16}, Matthew A. Malkan ¹⁷, Anthony H. Gonzale ^{1,10}, Matthew A. Malkan ^{1,10}, Guillaume Mahle ^{1,5,16}, Matthew A. Malkan ^{1,10}, Matthew A. Malkan ^{1,10}, Matthew A. Malkan ^{1,10}, Guillaume Mahle ^{1,5,16}, Matthew A. Malkan ^{1,10}, Guillaume Mahle ^{1,5,16}, Matthew A. Malkan ^{1,5}, Matthew A. Malkan Matthew A. Malkan ^{1,5}, Matthew Desika Narayanan Grace M. Olivier, Kedar A. Phadke, Cassie Reute, Jane R. Rigbo, J. D. T. Smith, Desika Narayanan, Spirit Reute, Manuel Soliman6², Nikolaus Sulzenaue³, Joaquin D.Vieira^{19,20,2}, David Vizgan¹⁹, and Axel Weise³ ¹Department of Physics and Astronomy and George P. and Cynthia Woods Mitchell Institute for Fundamental Physics and Astronomy, Texas A&M University, 424 TAMU, College Station,TX 77843-4242,USA; ² Observational Cosmology LalQode 665,NASA Goddard Space Flight Cente8800 Greenbelt RoadGreenbelt,MD 20771, USA ³ Department of AstronomyUniversity of Maryland,College Park,MD 20742, USA ⁴ Center for Research and Exploration in Space Science and Technology A/GSFC, Greenbelt MD 20771, USA ⁵ Instituto de Estudios Astrofísicos, acultad de Ingeniería y Ciencials niversidad Diego Portales, y Ejército 441, Santiago, Chile Department of Physics University of Cincinnati, Cincinnati, OH 45221, USA Department of AstronomyUniversity of Florida,211 Bryant Space Sciences Cent@ainesville,FL 32611 USA ⁸ Department of Physics and Astronomyniversity of British Columbia,6225 Agricultural Road, Vancouver V6T 1Z1, Canada National Research Councillerzberg Astronomy and Astrophysics 71 West Saanich Road/ictoria V9E 2E7, Canada 10 Department of Physics and Atmospheric Scien**De**lhousie University 6310 Coburg Road B3H 4R2 Halifax, Canada Department of Physics and Astronomy "Augusto Righi" (DIFA)niversity of Bologna, Via Gobetti 93/2, I-40129 Bologna, Italy INAF—Osservatorio di Astrofisica e Scienza dello Spazioa Gobetti 93/3, I-40129 Bologna, taly ¹³ Center for Computational Astrophysics 2 Fifth Avenue, New York, NY 10010, USA ¹⁴ Department of Physics and Astronomy and PITT PACOniversity of Pittsburgh,PA 15260,USA Centre for Extragalactic Astronom/Durham University South Road Durham DH1 3LE, UK ¹⁶ Institute for Computational Cosmolog Qurham University, South Road Durham DH1 3LE, UK ¹⁷ Department of Physics and Astronomyniversity of California, Los Angeles, 430 Portola PlazaLos Angeles, CA 90095, USA Cosmic Dawn Center at the Niels Bohr Institute inversity of Copenhagen and DTU-Space, chnical University of Denmark Department of Astronomy University of Illinois, 1002 West Green Street Irbana, IL 61801, USA ²⁰Center for AstroPhysical SurveyNational Center for Supercomputing Application 205 West Clark Street Urbana, IL 61801, USA University of Toledo Department of Physics and Astronon Ritter Astrophysical Research Centeroledo, OH 43606, USA 22 Instituto de Estudios Astrofísicos acultad de Ingeniería y Ciencial niversidad Diego Portale Avenida Ejército Libertador 441 Şantiago 8370191 Çhile
23 Max-Planck-Institut für Radioastronomi Auf dem Hügel 69, D-53121 Bonn, Germany ²⁴Department of PhysicsUniversity of Illinois, 1110 West Green StreetUrbana,IL 61801, USA; jbirkin@tamu.edu Received 2023 June 5; revised 2023 August 21; accepted 2023 August 24; published 2023 December 5

Abstract

We present the first spatially resolved maps of gas-phase metallicity for two dust-obscured star-forming galaxies at z ~ 4, from the JWST TEMPLATES Early Release Science prograderived from NIRSpec integrafield unit spectroscopy of the Hα and [N] emission lines. Empirical optical line calibrations are used to determine that the sources are globally enriched to near-solar levels. While one source shows elew attending and broad Hα emission consistent with the presence of an active galactic nucleus in a \(\square\$1 kpc region, we argue that both systems have already undergone significanthetal enrichmentas a result of their extremely high starformation rates. Utilizing Atacama Large Millimeter/submillimeterArray rest-frame 380 μm continuum and [Φ³P₂–³P₁) line maps we compare the spatial variation of the metallicity and gas-to-dust ratio in the two galaxies, finding the two properties to be anticorrelated on highly resolved spatial scales, consistent with various literature studies of z ~ 0 galaxies. The data are indicative of the enormous potential JWST to probe the enrichment of the interstellar medium on ~kpc scales in extremely dust-obscured systems at z ~ 4 and beyond.

Unified Astronomy Thesaurus concepts: Galaxy evolution (594); High-redshift galaxies (734); Galaxy formation (595); Starburst galaxies (1570); Strong gravitational lensing (1643)

1. Introduction

fraction of the Universe's star formation occurs in dustobscured star-forming galaxie \$DSFGs; Casey et al. 2014; Swinbank etal. 2014; Dudzevičiūtė etal. 2020; Zavala etal.

Original content from this work may be used under the terms of the Creative Commons Attribution 4.0 licence. Any further distribution of this work must maintain attribution to the author(s) and the title of the work, journal citation and DOI.

2021). In such systemsthe majority of the rest-frame optical At so-called "cosmic noon" (z ~ 2) and beyond, a significant and ultraviolet (UV) light associated with young stars is absorbed by dust and reprocessed into the far-infrared.

Multiwavelength analyses and moleculagas observations have revealed that DSFGs are massive, gas rich and highly star forming, with IR luminosities $L_{\rm IR}$ > 10¹² $L_{\rm e}$, implied star formation rates (SFRs) of 100–1000 $M_{\rm e}$ yr⁻¹ (see, e.g., Swinbank et al. 2014; Spilker et al. 2015; Aravena et al. 2016; Strandetet al. 2017; Dudzevičiūtė etal. 2020; Reuteret al. 2020; Birkin et al. 2021) and dense interstellar media (ISMs; e.g., Spilker et al. 2014; Birkin et al. 2021; Rybak et al. 2022; Reuter et al. 2023). The observed properties of DSFGs (such as

²⁵ NASA Postdoctoral Fellow.

their high IR luminosities) and the fact that sources have been detected up to z ~ 7 has made them challenging to reproduce in Summary of the Key Properties for Both DSFGs Studied in This Work current models of galaxy formation and evolution (Davé et al. 2010; Lacey et al. 2016; McAlpine et al. 2019; Hayward et al. 2021; Bassiniet al. 2023). Therefore, observations of DSFGs can provide strong constraints on such theories.

The ISM plays a critical role in the ongoing processes within DSFGs, such as star formatiosupernovae, and winds, which add, remove, and redistribute metals. Therefore, measuring th gas-phase metallicity and its variation across the galaxy is a powerful indicator of its past evolution (e.g., Maiolino & Mannucci 2019), for example through scaling relations such as the mass-metallicity relation (MZR; e.g., Tremonti et al. 2004) and fundamentalmetallicity relation (FMR; e.g., Mannucci et al. 2010; Curti et al. 2020). A simple and effective method for estimating metallicity is to measure the relative strengths of the [N II] and Hα emission lines (e.g., Pettini & Pagel 2004; Marino et al. 2013; Dopita et al. 2016; Maiolino & Mannucci 2019), which suffer similar levels of dust extinction due to their close proximity in wavelength. This method has limitations, such as being highly sensitive to the ionization parameter and N/O abundance (Pérez-Montero & Contini 2009; Dopita et al. 2016; Pilyugin & Grebel 2016; Peng et al. 2021), but the brightness of these lines and their accessibility at high redshifts Notes. Magnification values are taken from Cathey et al. (2023) for SPT0418-baye made them popular observable for metallicity (e.g., 47 and Spilker et al. (2016) for SPT2147-50. The SFRs, stellar masses and have made them popular observables for metallicity (e.g., Steidel et al.2014; Sanders et a2015; Gillman et al.2022).

The launch of JWST and its successfulcommissioning (Rigby et al. 2023a, 2023b; Gardneret al. 2023; McElwain et al. 2023; Menzel et al. 2023) have transformed our ability to significant than the uncertainties on our line ratio measurements. study galaxy formation and evolution, and we are now entering a new era for extragalactic astronomy!WST's Near-Infrared Spectrograph (NIRSpecBöker et al. 2023) can study highredshift galaxies atsub-kpc spatiaresolution, offering a vast improvement over previous ground-based(and therefore seeing-limited) studies. Additionally, at high redshifts the spectralcoverage of NIRSpec encompasses the key emission lines that trace gas-phase metallicity such as Holl 16584, [Ο ΙΙΙ] λλ5007, 4958, Ηβ, [SIΙ] λλ6717, 6731, [ΟΙΙ] λλ3727, 3729 and [Neii] λ3870 (e.g., Wuyts et al. 2014; Maiolino & Mannucci 2019; Sanders et 2020).

At high redshiftsstrong gravitational bensing due to massive foreground structures llows us to observe galaxies thigher spatial resolution than would otherwise be possible. This technique TES; Program 1355; PI: J. Rigby; Co-PI: J. Vieira). From is commonly used to study the DSFG population ith modest samples of lensed sources characterized by Herschel, Planck, the ervations of two SPT-selected DSFGsSPT0418-47 and Atacama Cosmology Telescope (ACT), the South Pole Telescope T2147-50. From spectral energy distribution (SED) fitting it (SPT; e.g Negrello et al. 2010; Vieira et al. 2013; Marsden et als known that both galaxies are highly massive and highly star 2014; Bussmann et al. 2015; Harrington et al. 2016; Spilker et Hrming (Cathey et al2023; see Table 1). 2016; Everett et al. 2020; Kamieneski et al. 2023), and through the JWST data used in this manuscriptcan be found in Atacama Large Millimeter/submillimeter Array (ALMA) Cluster MAST at 10.17909/fdje-fq59. We reduce the data with the been detected up to z ~ 7 (e.g., Marrone et al. 2018; Reuter et aling calibration reference data system (CRDS) context 2020; Endsley et al. 2023).

In this work, we present Director's Discretionary Early Release Science (DD-ERS) NIRSpec IFU observations of two Rigby et al. (2023, in preparation) but here we describe how SPT-selected gravitationally lensed DSFG&PT0418-17 at with which we demonstrate the significant dvancements that JWST is already providing in our study of this population. The sigma clipping method we firstmask the galaxy and clip the observations carried outur data reduction methodand our

Table 1

	SPT0418-47	SPT2147-50
R.A.	04:18:39.67	21:47:19.05
Decl.	-47:51:52.5	-50:35:53.5
μ	29.5 ± 1.2	6.6 ± 0.4
η η _{μ SFR/Me} yr ⁻¹	3770 ± 545	4630 ± 230
μ M*/M _e	$(4.5 \pm 0.9) \times 10^{11}$	$(4.2 \pm 1.0) \times 10^{11}$
n e A _V	3.8 ± 0.1	2.5 ± 0.1
Z	4.2246(4)	3.7604(2)
is	Whole Source	
[N II]/Hα	0.43 ± 0.03	0.62 ± 0.04
[S II]/Hα	0.23 ± 0.01	0.24 ± 0.01
12 + log(O/H) _{M13}	8.57 ± 0.16	8.65 ± 0.16
of Z _{M13} / Z _e	0.8 ± 0.3	0.9 ± 0.3
	Masking [N II]/Hα > 0.5	
 ir [N II]/Hα	0.34 ± 0.02	0.53 ± 0.02
[S]/Hα	0.21 ± 0.01	0.23 ± 0.01
12 + log(O/H) _{M13}	8.53 ± 0.16	8.55 ± 0.16
Z _{M13} /Z _e	0.7 ± 0.3	0.7 ± 0.3

dust attenuations are derived from SED fitting with CIGALE (Cathey et al. 2023; K. A. Phadke et al. 2023, in preparation). Redshifts are taken from Reuter et al.(2020). For the 12 + log(O/H) calibrations, we quote the scatter of the M13 calibration (0.16 dex) as the uncertainty, which is much more

and discuss their implications. In Section 4 we summarize our findings. Throughout this paper we adopt the cosmology measured by Planck Collaboration et. (2020), i.e., flat with $\Omega_{\rm m}$ = 0.310 and H₀ = 67.7 km $\bar{\rm s}^1$ Mpc⁻¹, and a solar metallicity of $12 + \log(O/H) = 8.69$ (Asplund et al.2021).

2. Observations, Data Reduction, and Analysis 2.1. JWST

The JWST/NIRSpec observations are drawn from the DD-ERS program Targeting Extremely Magnified Panchromatic Lensed Arcs and Their Extended Star formation (TEM-TEMPLATES we utilize NIRSpec IFU G395M/F290LP

Lensing Survey (ALCS; e.g., Sun et al. 2022). Many sources havendard JWST pipeline (version 1.10.2; Bushouse et al. 2023) jwst_1089.pmap, with some modificationsFull details on the TEMPLATES data reduction will be provided in J. R. our process differs from the standard pipeling modify the z = 4.2246 and SPT2147-50 at z = 3.7604 (Reuter et al. 2020) outlier detection stage of the pipeline as we found that in some cases the default stage can remove real signal. In our alternate outline of this paper is as follows: in Section 2 we describe the background, and then perform the same process on layers of the galaxy of increasing signal-to-noise ratio (S/N) his layering analysis of the reduced data. In Section 3 we present the results as chosen to ensure that spaxels with weaker emission did not

affect the clipping of spaxels with strong emissionWe also to ALMA rest-frame 380 µm continuum data (see Section 2.2), for each galaxy. The [SII] doublet is shown with a double-These astrometric shifts were determined by comparing the coordinates of the central continuum source with Hubble Spacebut the S/N is insufficient to detect it in individual pixels. Telescope/WFC3 F140W imaging (Ma et al. 015).

0"5 resolution (as opposed to the originar of resolution). This is done to ensure consistency with existing ALMA data (see Section 2.2), which we use to derive maps of the dust and espectively. We detect continuum emission across the gas emission. To generate the 0 5 resolution NIRSpec cubes we convolve the original (0.1 pixel scale) cubes with a circular stellar continuum from the background DSFGs and light from Gaussian point-spread function (PSF) of FWHM # 0 49. The sufficiently poorer than the intrinsic JWST PSF."(0 1) that the wings and spikes in the JWST PSF can be safely ignored.

2.2. ALMA

To supplement the data from JWST/NIRSpec, we utilize ALMA data covering the rest-frame 380 µm continuum emission and the $[C_1](^3P_2-^3P_1)$ line emission, which will be used in Section 3.3 as proxies for dust mass and gas mass, respectively. For SPT0418-47we utilize Band 4 data from program 2021.1.00252.S (PlJ. Vieira), which we image using natural weighting and taper to a spatial resolution of 0.5, creating continuum images and CO(7-6)/[(2-1) cubes. For SPT2147-50 we utilize Band 5 data from program 2018.1.01060.S (PI: J. M13): Vieira) which is processed in the same way, except the imaging was performed using Briggs weighting with a robust parameter of 0.45. This enabled us to achieve the same resolution as the SPT0418-47 data.

2.3. Resolved Fitting

To achieve our goal of determining how the metallicity varies across ourtwo targets, we model the Hα and [N II] complex as a triple-Gaussian profile, on a pixel-by-pixel basis, tying the wavelengths of the emission and coupling their line widths, with the $H\alpha/[N \parallel]$ flux ratio left as a free parameter. The flux ratio of $[N II] \lambda 6584/[N II] \lambda 6548$ is fixed at 2.8 (Osterbrock & Ferland 2006) and we also include a constant in each pixel, and if we measure an S/N of at least eight acrossmetallicities than C20who used a fourth-order polynomial fit the $H\alpha+[N \parallel]$ complex the pixel is included in the flux maps. Otherwise, the pixel is ignored, and not used in our subsequentan alternative measurementive briefly discuss results using analysis. The threshold of S/N = 8 was chosen through trial and error, to minimize pixels where the apparent Hα emission is largely due to noise while ensuring that the derived flux maps herefore for consistency we primarily use the M13 calibracontain enough pixels to study the resolved properties. To along with the fits to each spaxel, and mask by hand any spaxels where the emission does not appear to be coming from alues. the target galaxy. This includes masking emission from a newly As the [NII]/Hα ratio is very high (>0.8) in several regions detected companion galaxy (Peng et 2022: Cathey et al. of both sources, we cannot rule out active galactic nuclei detected companion galaxy (Peng et l. 2022; Cathey et al. 2023; see Section 3.1), which we elect not to study in detail in this work.

3. Results and Discussion

Figure 1 shows the 1D spectra extracted from the two DSFGs in pixels where Hα and [N II] are detected, and Figure 2 shows the same spectra, but this time zoomed into the 2016; Apostolovski et al. 2019). Therefore, this is a surprising

 $H\alpha$, $[N \parallel]$, and $[S \parallel]$ lines. We show both the integrated applied a small offset (40.5 for both sources) to match the dataspectra, and a sample spaxel (binned with neighboring spaxels) Gaussian fitin the integrated spectra as its clearly detected. Therefore we do not model [SII] in our resolved fitting. As part of our analysis we also generate NIRSpec cubes with the triple-Gaussian fit models the Hα and [N lines well in both cases. The resultant maps of Hα and [NII] emission are shown in Figures 3 and 4 for SPT0418-47 and SPT2147-50, observed wavelength range in both sourcescombination of the bright foreground lenses blurred into the background target spatial resolution (0 5, and Gaussian by construction) is emission by the JWST PSF. We model the continuum using a running median with a window size large enough so as to avoid removing any flux from the emission lines (~10,000 km¹). Both DSFGs display strong Hα and [N II] λ6584 emission, along with the [S_{II}] λλ6717, 6731 and [S_{III}] λλ9071, 9533 doublets. Additionally, in the lower-redshift SPT2147-50 we detect He and Pay emission with tentative evidence for Paδ.

3.1. Line Ratios and Metallicities

To derive metallicities for the two DSFGs we firstonvert the [N II] λ 6584/H α ratio from the line fits to an oxygen abundance12 + log(O/H) using the calibration for N2 = $\log_{10}([N II]/H\alpha)$ as derived by Marino et al. (2013; hereafter

$$12 + \log(O/H)_{M13} = 8.743 + 0.462 \text{ N2},$$
 (1)

which is derived from a fit to 452 H II regions with T_e-based metallicity measurementsThe regions considered are valid up to N2 = -0.2 or [N II]/H $\alpha \sim 0.63$. A number of other calibrations were considered, including those proposed by Pettini & Pagel (2004; hereafterPP04), Curti et al. (2020; hereafterC20) and Dopita et al. (2016; hereafterD16), the latter of which also uses the | Bdoublet. We selected the M13 calibration as it is considered more reliable at high redshifts and in better agreement with other calibrations than PP04 (e.g., continuum component. We attempt to model the emission lines Poetrodjojo et al. 2021), and is simpler to extrapolate to higher which is not well constrained in the high-metallicity regime. As the D16 calibration, but as the S/Ns of our [State ctions are low we are unable to use this line on a spatially resolved basis. tion. We note here that while we later study the globaMZR spaxels. Finally, we visually inspect the resultant Hα flux maps and FMR, our main concern in this work is the spatial variation of the metallicity with other properties rather than their absolute

> (AGN) as being responsible for this emissidn. SPT2147-50 this is supported by very broad FWHMs (~800 km)swhich correspond with regions of high [N $\,\textsc{II}$]/H α . This could be evidence for AGN-driven winds in this systemNo previous work on these two sources has suggested that either are AGN hosts (e.g., Bothwell et al. 2017; De Breuck 2019). The same is true for other DSFGs from the same parent sample (Maalet

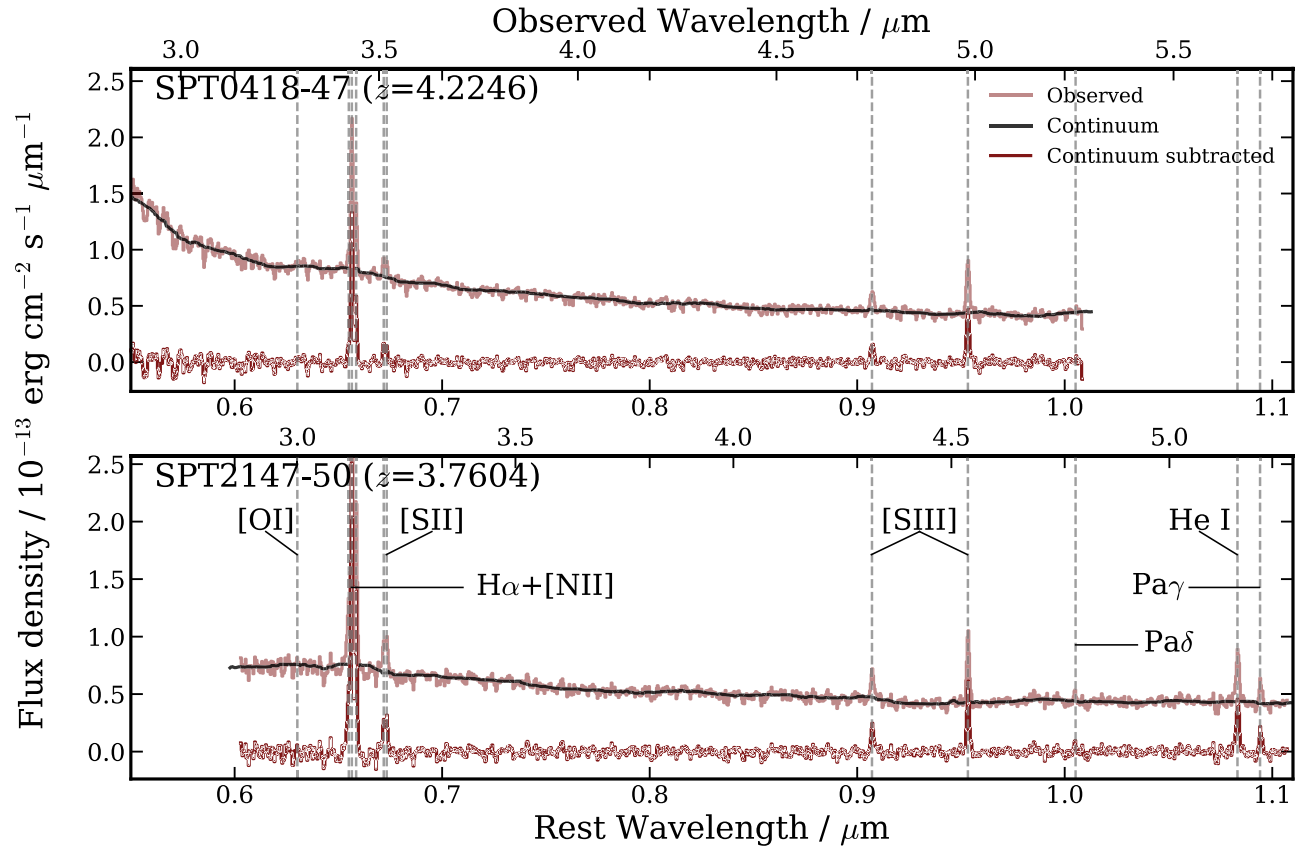


Figure 1. One-dimensional JWST/NIRSpec rest-frame spectra of SPT0418-47 and SPT2147-50, displaying strong detections of the Hamistibh lines, in addition to the [SII] doublet. Both spectra are extracted only from spaxels where HaHIN detected with S/N > 8. SPT2147-50 displays detections of the He line and Paγ linesand marginal evidence for Paδ emissioneither of the sources are detected in [D

result, particularly for SPT2147-50 which shows the highest [N II]/Hα ratios.

Galaxies are commonly classified as AGN dominated or otherwise using the Baldwin, Phillips, and Terlevich (BPT; Baldwin et al. 1981) diagram (e.g., Kewley et al. 2006). However, the other BPT diagnostics [C] and Hβ (neither of which fall within the coverage of our data) are needed to confirm this. Even with these additional diagnostics, the boundary between star-forming galaxies and AGN in the two DSFGs reside (Kewley et al. 2013). We therefore also derive metallicities masking ouindividual pixels with [N II]/ $H\alpha > 0.5$, which we choose to provide a conservative lower limit on the integrated metallicity.

In the former case, i.e., using all pixels with Hα detections, and based on the M13 calibration\$PT0418-47 has 12 + log e, respectively. $(O/H) = 8.57 \pm 0.16$ and $Z = 0.8 \pm 0.3$ Z SPT2147-50 has 12 + $\log(O/H)$ = 8.65 ± 0.16 and Z = 0.9 ± 0.3 Z_e, respectively Adopting a conservative cutoff of [N]/ $H\alpha > 0.5$ (which masks ~43% and ~ 70% of the pixels in SPT0418-47 and SPT2147-50, respectively) these values change to Z = $0.7 \pm 0.3 Z_e$ for SPT0418-47 and Z = $0.7 \pm$ 0.3 Ze for SPT2147-50Interestingly, applying this correction does not significantly change the global metallicity values; bothlines in our analysis. are still a significant fraction of the solar value, and consistent with solar abundances in all cases.

The detections of [S] λλ6717, 6731 are significant enough in the integrated spectra of both galaxies (see Figure 2) to provide an independent stimate of the metallicity. Additionally, [SII] is sufficiently close in wavelength to H α and [N]

that any extinction corrections would be negligible. We therefore also apply the D16 calibration for H α , [N II], and [SII] to estimate 12 + log(O/H). Interestingly, this calibration gives significantly higher values of metallicity: Z = 1.8 ± $0.7 \, Z_{\rm e}$ for SPT0418-47 and $Z = 2.7 \pm 1.0 \, Z_{\rm e}$ for SPT2147-50 (decreasing to 1.5 \pm 0.6 Ze and 1.7 \pm 0.7 Ze, respectively, when applying our AGN masking). The D16 calibration has been claimed to have a reduced dependence on the ionization parameter when compared to Nand therefore this is further BPT diagram is uncertain at $z \sim 2$, let alone at $z \sim 4$ where the evidence that the two DSFGs are highly enriched with metals, possibly even to solar or super-solar levels.

We note that the two [8] lines that we detect here can also be used to trace the ionization parameter and metallicity. There remains uncertainty over the reliability of NIRSpec flux calibrations as a function of wavelengthand so we prefer to only use ratios between emission lines that are close in wavelength Additionally, we would require the application of extinction corrections to our datagiven the large wavelength difference between [\$1] and the other lines. As we do not have measurements of the Hβ fluxand therefore the Balmer decrement, our extinction corrections would be highly uncertain. Therefore we have elected not to use the [S III]

As a side note, a companion source to SPT0418-47 SPT0418-47B) has been detected by Pengæt (2022) and Cathey et al. (2023). While we are not focused on the nature of this source here, we note that we measure a metallicity of ~0.6-0.7 Z_e (applying the M13 calibration), which we find to be consistent with Peng et al. (2022). Therefore the smaller

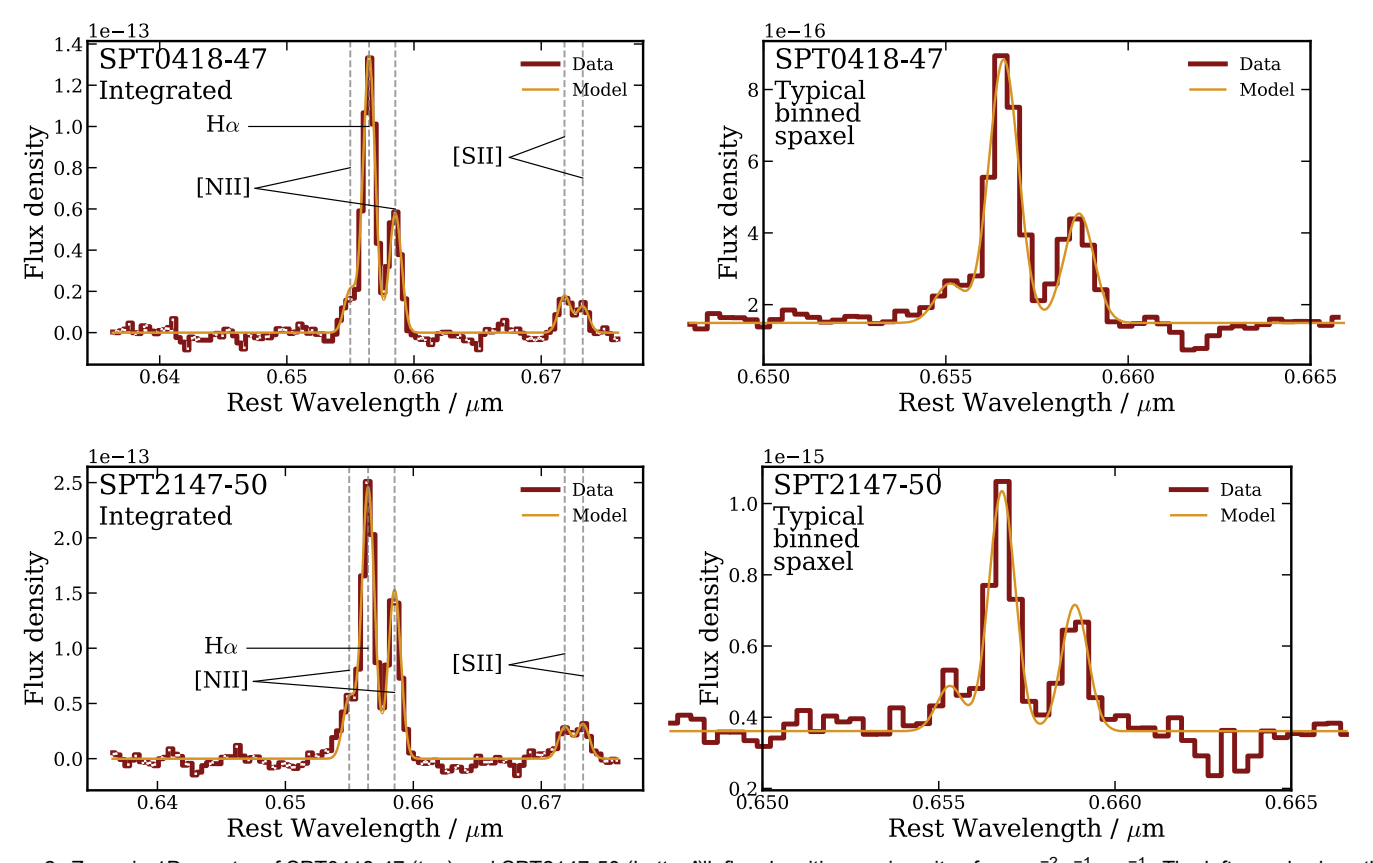


Figure 2. Zoom-in 1D spectra of SPT0418-47 (top) and SPT2147-50 (bottonANI flux densities are in units of erg cm² s⁻¹ µm⁻¹. The left panels show the integrated spectra, and the right panels show a sample typical 3 × 3 binned spaxel, as used in the spatially resolved fitting. The emission lines are well modeled by Gaussians. We note that the integrated spectra are fit here with \$2shown in the plot, but for the binned spaxels we only fit Ha and the [thoublet, as [Si] is typically too faint to be significantly detected in individual binned spaxels.

merging companion to SPT0418-47 is a slightly less metal-richhas been suggested and named the fundamenta Metallicity system.

may arise from diffuse ionized gas (DIG), as the resolution of our observations is much greater than the scale of individual HII regions. Vale Asari et al. (2019) investigated this effect for star-forming galaxiesin the MaNGA survey and found the diffuse component to have a ~0.1 dex contribution to metallicity estimates derived using the **IN** Hα index, at the high-metallicity end. They also found the DIG to have a more prominent effect on the MZR at the high-stellar-masænd, where our sources (particularly SPT2147-50) lie. Similar findings were also made by Poetrodjojo et al. (2019). A correction for this potential effect is beyond the scope of this work. however.

calibrations and the facthat these are derived for galaxies at much lower redshifts than the two SPT DSFGsjt is highly challenging to constrain their globalmetallicities confidently. However, even while being conservative over the possibility of AGN emission in the two DSFGs, we can confidently say that both are enriched to near-solar levels, likely as a result of their and are shifted horizontally for visual clarity. very high SFRs.

3.2. MZR and FMR

phase metallicity and stellar matter so-called mass-metallicity relation (MZR; e.g.Tremonti et al2004). In addition, a "threedimensional" relation between stellar manestallicity, and SFR

Relation (FMR;Mannucciet al. 2010). In the FMR, low-mass A potential source of uncertainty in our metallicity estimates galaxies with higher SFRs typically contain a lower proportion of metals, and in high-mass galaxies the metallicity saturates and becomes independentSFR (as in the MZR)Mannucciet al. (2010) found this relation to hold constant with low scatter up to z ~ 2.5 (also seee.g., Lara-López etal. 2010; Troncoso etal. 2014; C20), attributing the result to the dominance and consistency of smooth secular processes watto intermediate redshifts, with this equilibrium being reached atteast as early as z ~ 2.5.

At higher redshifts the picture is less cleamannucciet al. (2010) showed that galaxies at $z \sim 2.5$ are offset from the FMR, specifically around 0.6 dex toward lower metallicities, which may imply that smooth secular processes are less prominent in higher-In general, due to the systematic uncertainties in the different edshift sources. To test this for the two z ~ 4 DSFGs, in Figure 5 we show the derived oxygen abundances $12 + \log(O/H)$ using the C20 calibration versusstellar massesderived from SED fitting with CIGALE (Cathey et al. 2023; K. A. Phadke et al. 2023, in preparation). The open points indicate the oxygen abundances derived from masking emission in pixels with $[N]H\alpha > 0.5$,

For comparison with other similarly selected sources, we also include in Figure 5 z \sim 2 DSFGs with $[N]/H\alpha$ measurements from the K-band Multi-Object Spectrograph (KMOSBirkin In general, galaxies appear to display a correlation between algebra, along with z ~ 1.3-2.6 galaxies from the KMGG vey (Wisnioski et al. 2015), the latter of which is generally comprised of galaxies with lower SFRs than those studied in this work. The two DSFGs presented in this work are consistent with the

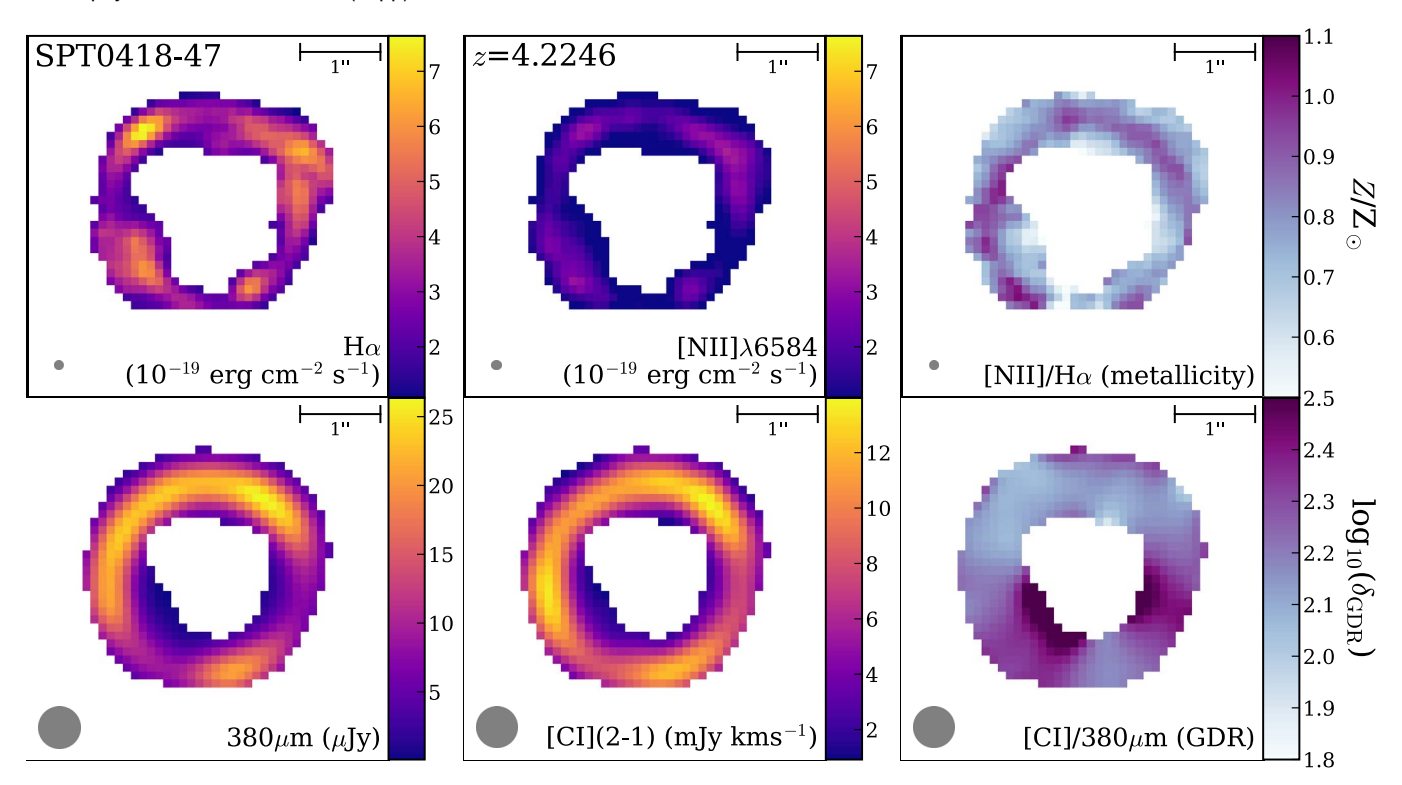


Figure 3. Top row: resolved H α , [N II], and [N II]/H α maps of SPT0418-47 from JWST/NIRSpec (lefto right). The [N II]/H α map is used as a proxy for metallicity. Bottom row: ALMA rest-frame 380 μ m continuum and][Ω e maps, along with the resultantI[Ω 80 μ m map (left to right). The [Ω /380 μ m map is used as a proxy for the gas-to-dust ratio. The gray circles show the approximate PSF of the data in each panel, and the horizontal bars in the top right of each pan indicate the scale of 1" (~0.7 kpc at z = 4).

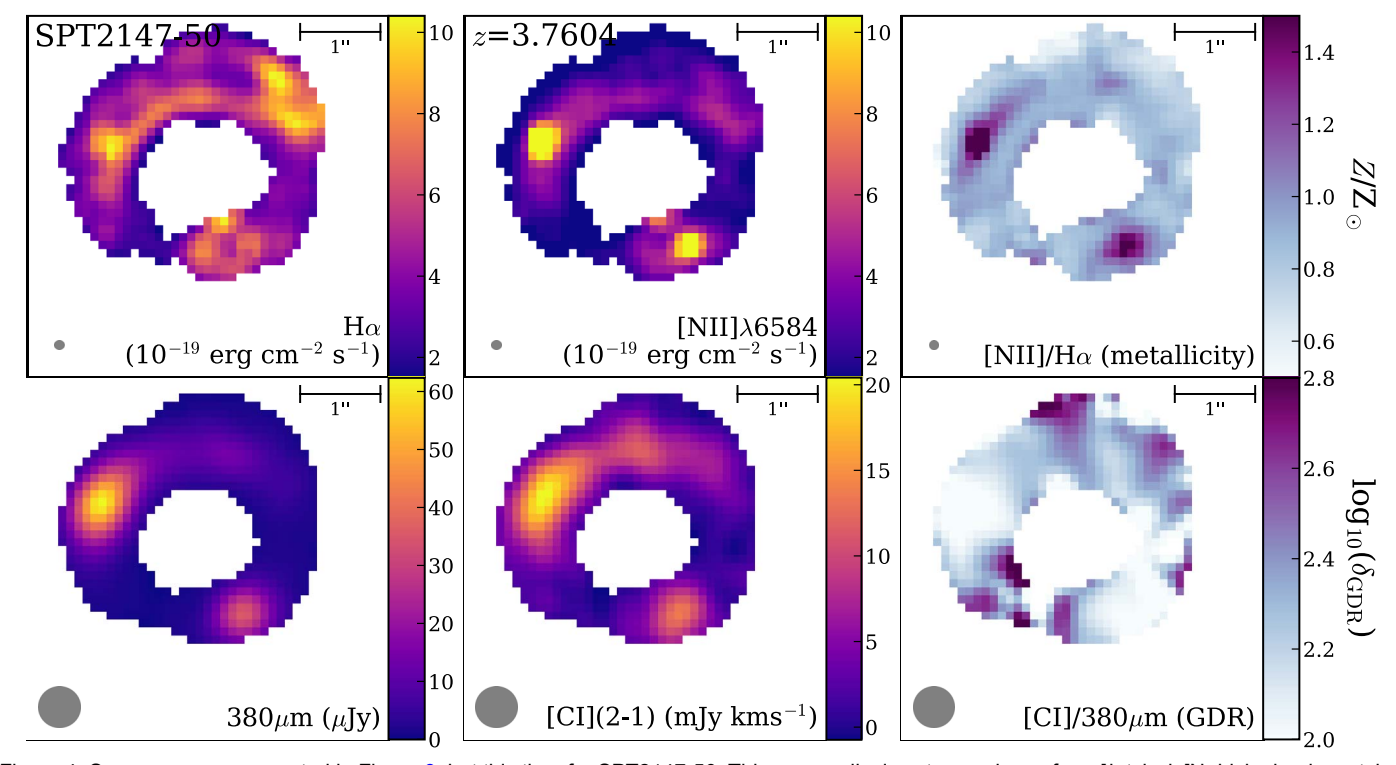


Figure 4. Same maps as presented in Figure 3, but this time for SPT2147-50. This source displays two regions of verty] ietreissio [Nwhich clearly match with regions of strong rest-frame 380 µm and clive galactic nucleus (AGN).

majority of the comparison sources, albeit generally on the more cluding the scatter in both cases. Both galaxies are consistent metal-rich end.

with the local MZR within the uncertainties—they are high-

From C20 we show the MZR for local galaxies ong with the FMR for the SFRs of the two galaxies (see Table 1),

with the local MZR within the uncertainties—they are highmass galaxies at which point the metallicity is expected to saturate at around 12 + log(O/H) ~ 8.7–8. According to the

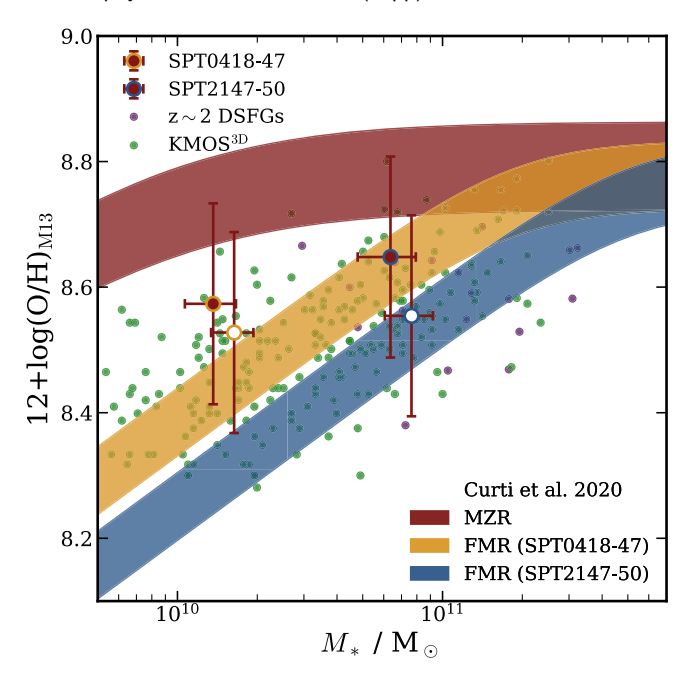


Figure 5. Oxygen abundance 12 + log(O/H)estimated from the [NII]/Hα ratio, using the M13 calibration (see Section 3.1),s. stellar mass estimated from SED fitting. As comparison sampleswe include galaxies from the KMOS^{3D} survey (Wisnioski et al. 2015), and z ~ 1.5-2.5 DSFGs also observed with KMOS (Birkin 2022). From C20 we display the MZR (red shaded) and the FMR for the SFRs of the two galaxies (yellow for SPT0418-47, blue for SPT2147-50). The open points show how fardown the points would move if we were to exclude pixels with $\ln H = 0.5$ conservatively to account for AGN (the points are also shifted horizontally for visual clarity). Both DSFGs are consistent with the MZR, and are also consistent with the upper end of the FMR, particularly when we account for potential AGN emission.

FMR they are both marginally more metal rich than expected, although generally consistent within the large uncertainties. especially when we account for potential AGN emission.

Mannucci et al. (2010) claim that the relatively small scatter in the FMR up to $z \sim 2.5$ implies constant relative significance of star formation and infall and outflows of gas. The two galaxies presented in this papeappearto have metallicities consistentwith the FMR and could therefore fit into this picture. However, SPT0418-47 seems to be interacting with a be expected to drive it away from the FMR. Studies using both Figure 2 and 4 to drive it away from the FMR. observations and simulations have shown that in the early stages of a merger the gas is diluted, thus lowering the metallicity. Subsequentlythe metallicity is increased as the merger proceeds, when the SFR is enhanced (e.g., Rupke et alatio, which we use as a proxy for the gas-to-dust ratio \hbar 2008; Montuori et al.2010; Rupke et al. 2010). It is therefore interesting that SPT0418-47 remains consistent with the FMR. regions of high [Nι]/Hα coinciding with regions of high flux We choose not to overinterpret this result given the large uncertainties on the oxygen abundances.

We note that we use the relations from C20 as M13 do not derive either the FMR or the MZR from their calibration. these relations were available for the M13 calibratioand if anything this would place the two DSFGs ~0.2 dex further above the FMR than we see in Figure 5 his would put both sources firmly above the FMR.

An important consideration to make is whether or nother line calibrations we assume are applicablezat 4. There are few T_e-method-based metallicity measurements calibrated to

Hα and [NII] at this epoch (although some work has been done with Hβ and [OIII]; e.g., Curti et al. 2023; Trump et al. 2023), hence our reliance on local calibrations, and it is possible DSFGs exhibit different relative abundances than nearby galaxies. For instance, a top-heavy initial mass function, as has been suggested as necessary to reconcile DSFG number counts with theory (e.g., Baugh et al. 2005), and therefore a large number of high-mass stars, would lead to a change in the relative abundances of nitrogen, oxygen, and hydrogen, A lack of observational data limits our ability to draw the correct conclusion, however some work on this topic has already been done with NIRSpec. For example, for z = 2.18 galaxies Sanders etal. (2023) have found evidence thathe local C20 N2 calibration for metallicity is biased ~0.5 dex high when compared to direct measurements from auroral lines. This bias may be as significant protentially even worse $z \sim 4$.

A further consideration is thatif SPT2147-50 does in fact host an AGN that is contributing significantly to the IR emission, then this could result in a larger estimate of the SFR from SED fitting than the true value. This would in turn mean that the expected metallicity from the FMR is actually lower than it should be. Additionally, the SFRs used in the C20 scaling relations are derived from Hα luminosities, scaled to a total SFR. Given the high levels of dust extinction in the two galaxies (see Table 1), we do not derive Hα-based SFRs in this work, as the corrections are likely to be significant and uncertain. We instead use total SFRs derived from CIGALE SED fitting, which uses the parameterization from Boquien et al. (2019), with the star formation histories modeled as an exponential decay (Tirst = 1 Gyr) including an additional burst component using the stellar population model from Bruzual & Charlot (2003).

Resolved Metallicities and the Gas-to-dust Ratio

The impressive sensitivity and resolution of JWST has allowed us to resolve the [NII]/Hα flux ratio spatially (see Figures 3 and 4). We wish to compare these with the distribution of dust and gas in the two galaxies in order to determine how they are related. We therefore compare the [N II]/Hα maps from NIRSpec with existing ALMA imaging of the rest-frame 380 µm continuum and [0] line emission,

Figures 3 and 4 show ALMA rest-frame 380 µm continuum maps and [C] emission line maps of the two DSFGs, the latter of which are derived by summing the flux within twice the FWHM of the line. We also show maps of the IDo 380 µm Visually, these three maps are broadly consistent terms of in the ALMA maps. This is most clear in SPT2147-50, which displays two brightregions in the 380 µm maps thater also present in the NIRSpec data.

To quantify the relation between the metallicity, gas, and However, we note that we would expect both to move down if dust, we convert the ALMA maps to dust and gas mass surface density Σ_{dust} and Σ_{gas} and plot both versus [NII]/H α on a pixel-by-pixel basis, as shown in Figure 6. To convert the ALMA rest-frame 380 µm continuum maps to dust mass maps we apply Equation (1) of Dunne et al. (2003), assuming a dust mass opacity coefficientat 125 µm of 2.64 m² kg⁻¹, a dust temperature Just of 40 K, and extrapolating to 380 µm with dust emissivity index β = 2.0.

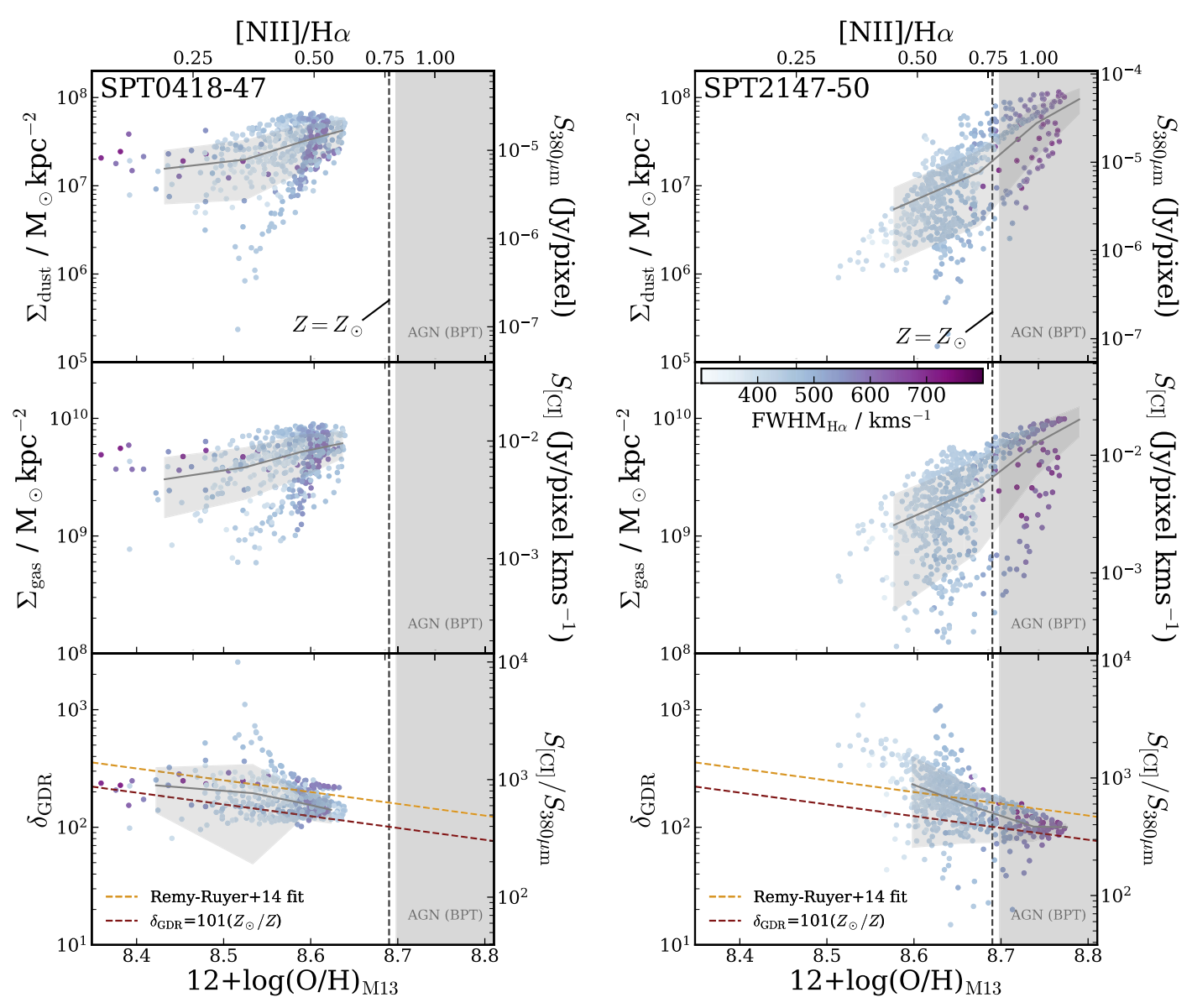


Figure 6. Spaxel-by-spaxel (0 1, ~ 0.7 kpc) variation of 380 μm flux (top), (Cine flux (middle), and [Q]/380 μm flux ratio (bottom) as a function of [N]/Hα line ratio for the two SPT DSFGs. On the top axes we show the corresponding oxygen abundances according to the calibration of M13. On the right axes we show corresponding dust mass surface density agas mass surface density and gas-to-dust ratio be using the conversions described in Section 3.3. We plot a binned median (gray line) with 1σ scatter (gray region), and color code points by Hα FWHM. We also indicate solar metallicity (Asplund et al. 2021) and shade the region where [Ni]/Hα > 0.8, the latter of which is likely to be contaminated to some extent by AGN emission. Notably, in this region Hα emission is broadest when compared to the resbf the source. In both sources the gas-to-dusatio appears to decline with increasing metallicitalthough this trend is more prominent SPT2147-50In the bottom panels we also show models from Rémy-Ruyer e(2014) and Aniano et al(2020), which are discussed further in Section 3.3.

This approach ignores any potential variations dig and β. However, Spilker et al. (2023) recently analyzed rest-frame 120nstead of the [C I](1-0) values. Following Papadopoulos & and 160 μ m data from SPT0418-47 and found no evidence of Significant variations in dust temperature across the sourde. abundance ratio of $X_{[CI]} = 3 \times 10^{-5}$. This is a commonly indeed we are seeing AGN emission in SPT2147-50 then we may expect these regions to display higher dustinperatures, but we flag regions of the parameter space in Figure 6 where this is likely to be the case and avoid overinterpreting these regions. There has yet to be significant study of variations in the dust emissivity across individual alaxies, and indeed we cannot rule this out in our sources.

To convert the [C I] emission line maps to moleculargas mass maps we use Equation (6)of Bothwell et al. (2017), exceptin our case we use the Einstein $A = 2.68 \times 10^{-7} \text{ s}^{-1}$

 $Q_{21} = 0.22$ (Dunne et al. 2022) for the [C I](2–1) transition cannot be measured for high-z galaxies and is therefore based on measurements from local galaxies. It is therefore subject to considerable uncertaintyIndeed, through a comparison with dust-based gas masses, Bothwell et al. (2017) suggested that a higher value of $X_{[CI]} = 7 \times 10^{-5}$ could also be reasonable. Given that we are primarily concerned with the variation of $\delta_{\!\mathsf{GDR}}$ with metallicity, $\,$ rather than its $\,$ absolute value, this assumption should not significantly affect our conclusions.

In Figure 6 we plot three quantities as a function of that, coefficient (Papadopoulos & Greve 2004) and excitation factor a proxy for metallicity. These are S_{380_m} , S_{CII} and S_{CII} , S_{380_m} , which we use as proxies for dust mass surface density, gas masse as proxies for dust and gas mass, respectively, we find that surface density, and gas-to-dust ratio, respectively. The points the gas-to-dust ratio is negatively correlated with the color coded by Ha FWHM. Given the various caveatsand assumptions which come with these proxies choose to plot both the observed and converted quantitieur interpretation will mostly focus on the variation of these properties rather than from $z \sim 0$ galaxies even on highly resolved spatial scales. their absolute values. Additionally, all corresponding panels are In the absence of [ΦI] and Hβ coverage we interpret these shown on the same scale (of absolute values) to enable a direct sults with caution as the possibility remains that gions of comparison between the two galaxieWe also indicate solar metallicity and shade the region where $IIMH\alpha > 0.8$, which the BPT diagram suggests is likely to result from AGN emissiomeconstruction of these data have not yet been carried out; this

First, we note that in both galaxies, there appears to be a positive correlation between dust/gas mass surface density and first resolved metallicity maps in DSFGs at z ~ and the metallicity. This indicates that regions containing more gas anddata quality shows the potential of JWST to further our dust are also more metal rich. This trend is stronger in SPT2147-50, in which we see that the most metal-rich regions redshift DSFGs. also display the broadest $H\alpha$ emission. Given that these points fall within the shaded regionit is likely that the most "metalrich" regions of SPT2147-50 aren fact regions of AGN emission. This is a striking conclusion given that no clear AGN PostdoctoraProgram (NPP) atNASA Goddard Space Flight including some objects more extreme than those targeted here. Center, administered by Oak Ridge Associated Universities (e.g., Ma et al. 2016; Apostolovski et al. 2019). It is theorized that DSFGs proceed to evolve through a quasi-stellarbject phase (Blain et al2002; Swinbank et al. 2006; Hopkins et al. 2008), and therefore we may be observing the beginnings of this evolution in SPT2147-50NIRSpec follow up should be proposed for other sources in the SPT DSFG samiplearder to identify any further AGN candidates.

Turning to the bottom panels, we see that the gas-to-dust ratio appears to decline with increasing metallicity, a result tha has been observed in locagalaxies (e.g.,Leroy et al. 2011; Rémy-Ruyeret al. 2014; Aniano et al. 2020). In the bottom panels of Figure 6 we plot two models to compare with our data. We show the modelfit by Rémy-Ruyer etal. (2014) to 126 local galaxies spanning ~2 dex in metallicity, derived from strong-line calibrations. Next we include a simple model from Aniano et al. (2020) in which the gas-to-dust ratio is estimated assuming that essentially all heavy elements are in dust grains under NASA contract NoNAS 5-03127. The National Radio with solar relative abundances. This results in a linear relation between metallicity and BR. Both models appear to match the results from both galaxies within the uncertainties/en if we ignore the absolute values the trend of decreasing δ_{DR} with metallicity is generally well described by both models. We tentatively conclude that the gas-to-dust ratio and its variation with metallicity in these two DSFGs is consistent with findings from local galaxies, which is not necessarily unexpected but has not yet been shown for DSFGs as distants the two we present in this paper.

4. Conclusions

We have presented two of the first spatially resolved metallicity maps of DSFGs at z ~ 4, utilizing IFU observations with JWST/NIRSpec. Both sources are detected in Hα and [N II] at very high S/N, enabling us to perform resolved spectroscopy of these lensed systems. We find both SPT0418-Taylor A. Hutchison® https://orcid.org/0000-0001-47 and SPT2147-50 to be enriched to near-solametallicity (conservatively ~0.7 ढ़), with evidence for AGN-like [NII]/ Hα ratios and broad Hα emission. The derived oxygen abundances are consistentith the FMR for both galaxies. Through a directcomparison with ALMA rest-frame 380 µm continuum and [C] line maps at matched resolution, which we

metallicity, a result that is consistent with literature studies of local galaxies. At least qualitatively, it appears that these early-Universe dusty galaxies bear some resemblance to expectations high $[N \parallel]/H\alpha$ are actually the result of AGN emission. Furthermore, detailed lens modeling analysis and source plane

will be explored in future work. Regardless, this work presents understanding ofthe processes that hape the ISM in high-

Acknowledgments

under contract with NASA. The SPT is supported by the NSF through grant OPP-1852617 J.D.V. and K.P. acknowledge support from the US NSF under grants AST-1715213 and AST-1716127.J.D.V. acknowledges supportrom an A. P. Sloan Foundation Fellowship J.S.S. is supported by NASA Hubble Fellowship grant No. HF2-51446 awarded by the Space Telescope Science Institute/hich is operated by the Association of Universities for Research in Astronomylnc., for NASA, under contractNAS 5-26555.D.N. acknowledges support from the US NSF under grant 1715206 and Space Telescope Science Institute under grant AR-15043.0001 M.A. acknowledgessupport from FONDECYT grant 1211951, ANID+PCI+INSTITUTO MAX PLANCK DE ASTRO-NOMIA MPG 190030, ANID+PCI+REDES 190194, and ANID BASAL project FB210003.JWST is operated by the Space Telescope Science Institute under the management of the Astronomy Observatory is a facility of the National Science Foundation operated undecooperative agreemently Associated Universities, Inc. This paper makes use of the following ALMA data: ADS/JAO.ALMA#2018.1.01060.S and ADS/ JAO.ALMA#2021.1.00252.S. ALMA is a partnership of ESO (representingits member states), NSF (USA) and NINS (Japan), together with NRC (Canada), MOST and ASIAA (Taiwan), and KASI (Republic of Korea) in cooperation with the Republic of Chile. The Joint ALMA Observatory is operated by ESOAUI/NRAO, and NAOJ.

Facilities: JWST and ALMA.

Software: astropy (Astropy Collaboration et al. 2018) and CASA (McMullin et al. 2007).

ORCID iDs

Jack E.Birkin https://orcid.org/0000-0002-3272-7568 6251-4988

Brian Welch https://orcid.org/0000-0003-1815-0114 Justin S.Spilker https://orcid.org/0000-0003-3256-5615 Manuel Aravena https://orcid.org/0000-0002-6290-3198 Matthew B. Bayliss https://orcid.org/0000-0003-1074-4807 Jared Cathey https://orcid.org/0000-0002-4657-7679

```
Anthony H. Gonzalez https://orcid.org/0000-0002-
0933-8601
```

Gayathri Gururajan https://orcid.org/0000-0002-7472-7697 Christopher C.Hayward https://orcid.org/0000-0003-

Gourav Khullar https://orcid.org/0000-0002-3475-7648 Keunho J.Kim https://orcid.org/0000-0001-6505-0293 Guillaume Mahler https://orcid.org/0000-0003-3266-2001 Matthew A. Malkan https://orcid.org/0000-0001-6919-1237

Desika Narayanan https://orcid.org/0000-0002-7064-4309 Grace M.Olivier https://orcid.org/0000-0002-4606-4240 Kedar A. Phadke https://orcid.org/0000-0001-7946-557X Cassie Reuter https://orcid.org/0000-0001-7477-1586 Jane R.Rigby https://orcid.org/0000-0002-7627-6551 J. D. T. Smith https://orcid.org/0000-0003-1545-5078 Manuel Solimano https://orcid.org/0000-0001-6629-0379 Nikolaus Sulzenaue https://orcid.org/0000-0002-3187-1648

Joaquin D.Vieira https://orcid.org/0000-0001-7192-3871 David Vizgan https://orcid.org/0000-0001-7610-5544 Axel Weiss® https://orcid.org/0000-0003-4678-3939

References

```
Aniano, G., Draine, B. T., Hunt, L. K., et al. 2020, ApJ, 889, 150
Apostolovski, Y., Aravena, M., Anguita, T., et al. 2019, A&A, 628, A23
Aravena, M., Spilker, J. S., Bethermin, M., et al. 2016, MNRAS, 457, 4406
Asplund, M., Amarsi, A. M., & Grevesse, N. 2021, A&A, 653, A141
Astropy Collaboration, Price-Whelan, A. M., & Sipőcz, B. M. 2018, AJ,
   156, 123
Baldwin, J. A., Phillips, M. M., & Terlevich, R. 1981, PASP, 93, 5
Bassini,L., Feldmann,R., Gensior,J., et al. 2023, MNRAS, 525, 5388
Baugh, C. M., Lacey, C. G., Frenk, C. S., et al. 2005, MNRAS, 356, 1191
Birkin, J. E. 2022, PhD thesis, Univ. Durham
Birkin, J. E., Weiss, A., Wardlow, J. L., et al. 2021, MNRAS, 501, 3926
Blain, A. W., Smail, I., Ivison, R. J., Kneib, J. P., & Frayer, D. T. 2002, PhR,
Böker, T., Beck, T. L., Birkmann, S. M., et al. 2023, PASP, 135, 038001
Boquien, M., Burgarella, D., Roehlly, Y., et al. 2019, A&A, 622, A103
Bothwell, M. S., Aguirre, J. E., Aravena, M., et al. 2017, MNRAS, 466, 2825
Bruzual, G., & Charlot, S. 2003, MNRAS, 344, 1000
Bushouse, H., Eisenhamer, J., Dencheva, N., et al., 2023 JWST Calibration
  Pipeline,v1.10.2 Zenododoi:10.5281/zenodo.7829329
BussmannR. S., Riechers D., Fialkov, A., et al. 2015, ApJ, 812, 43 Casey, C. M., Narayanan D., & Cooray, A. 2014, PhR, 541, 45
Cathey, J., Gonzalez A. H., Lower, S., et al. 2023, arXiv:2307.10115
Curti, M., D'Eugenio, F., Carniani, S., et al. 2023, MNRAS, 518, 425
Curti, M., Mannucci, F., Cresci, G., & Maiolino, R. 2020, MNRAS, 491, 944
Davé, R., Finlator, K., Oppenheimer, B. D., et al. 2010, MNRAS, 404, 1355
De Breuck, C. 2019, A&A, 631, A167
Dopita, M. A., Kewley, L. J., Sutherland, R. S., & Nicholls, D. C. 2016,
          .361,61
Dudzevičiūtė U., Smail, I., Swinbank, A. M., et al. 2020, MNRAS, 494, 3828
Dunne, L., Eales, S. A., & Edmunds, M. G. 2003, MNRAS, 341, 589
Dunne, L., Maddox, S. J., Papadopoulos, P. P., Ivison, R. J., & Gomez, H. L.
               AS, 517, 962
Endsley, R., Stark, D. P., Lyu, J., et al. 2023, MNRAS, 520, 4609
Everett, W. B., Zhang, L., Crawford, T. M., et al. 2020, ApJ, 900, 55
Gardner, J. P., Mather, J. C., Abbott, R., et al. 2023, PASP, 135, 068001
Gillman, S., Puglisi, A., Dudzevičiūtė, U., et al. 2022, MNRAS, 512, 3480
Harrington, K. C., Yun, M. S., Cybulski, R., et al. 2016, MNRAS, 458, 4383
```

```
Kamieneski, P. S., Yun, M. S., Harrington, K. C., et al. 2023, arXiv:2301.
                                                                                      09746
                                                                                   Kewley, L. J., Dopita, M. A., Leitherer, C., et al. 2013, ApJ, 774, 100
                                                                                   Kewley, L. J., Groves, B., Kauffmann, G., & Heckman, T. 2006, MNRAS,
                                                                                   Lacey, C. G., Baugh, C. M., Frenk, C. S., et al. 2016, MNRAS, 462, 3854
                                                                                   Lara-López,M. A., Cepa,J., Bongiovanni,A., et al. 2010, A&A, 521, L53
                                                                                   Leroy, A. K., Bolatto, A., Gordon, K., et al. 2011, ApJ, 737, 12
                                                                                   Ma, J., Gonzalez A. H., Spilker, J. S., et al. 2015, ApJ, 812, 88
                                                                                   Ma, J., Gonzalez A. H., Vieira, J. D., et al. 2016, ApJ, 832, 114
                                                                                   Maiolino, R., & Mannucci, F. 2019, A&ARv, 27, 3
                                                                                   Mannucci, F., Cresci, G., Maiolino, R., Marconi, A., & Gnerucci, A. 2010,
                                                                                      MNRAS, 408, 2115
                                                                                   Marino, R. A., Rosales-OrtegaF. F., Sánchez,S. F., et al. 2013, A&A,
                                                                                      559, A114
                                                                                   Marrone, D. P., Spilker, J. S., Hayward, C. C., et al. 2018, Natur, 553, 51
                                                                                   Marsden, D., Gralla, M., Marriage, T. A., et al. 2014, MNRAS, 439, 1556
McAlpine, S., Smail, I., Bower, R. G., et al. 2019, MNRAS, 488, 2440
                                                                                   McElwain, M. W., Feinberg, L. D., Perrin, M. D., et al. 2023, PASP, 135,
                                                                                      058001
                                                                                   McMullin, J. P., Waters, B., Schiebel, D., Young, W., & Golap, K. 2007, in
                                                                                      ASP Conf. Ser. 376, Astronomical Data Analysis Software and Systems
                                                                                      XVI, ed. R. A. Shaw, F. Hill, & D. J. Bell (San Francisco, CA: ASP), 127
                                                                                   Menzel, M., Davis, M., Parrish, K., et al. 2023, PASP, 135, 058002
                                                                                   Montuori, M., Di Matteo, P., Lehnert, M. D., Combes, F., & Semelin, B. 2010,
                                                                                   Negrello, M., Hopwood, R., De Zotti, G., et al. 2010, Sci, 330, 800
                                                                                   Osterbrock, D. E., & Ferland, G. J. 2006, Astrophysics of Gaseous Nebulae
                                                                                      and Active Galactic Nuclei (Mill Valley, CA: Univ. Science Books)
                                                                                   Papadopoulos, P., & Greve, T. R. 2004, ApJL, 615, L29
                                                                                   Peng,B., Lamarche,C., Stacey,G. J., et al. 2021, ApJ, 908, 166
Peng,B., Vishwas,A., Stacey,G., et al. 2023, ApJL, 944, L36
                                                                                   Pérez-Montero E., & Contini, T. 2009, MNRAS, 398, 949
                                                                                   Pettini, M., & Pagel, B. E. J. 2004, MNRAS, 348, L59
                                                                                   Pilyugin, L. S., & Grebel, E. K. 2016, MNRAS, 457, 3678
                                                                                   Planck Collaboration Aghanim, N., & Akrami, Y. 2020, A&A, 641, A6
                                                                                   Poetrodjojo,H., D'Agostino, J. J., Groves,B., et al. 2019, MNRAS, 487, 79
                                                                                   Poetrodjojo, H., Groves, B., Kewley, L. J., et al. 2021, MNRAS, 502, 3357
                                                                                   Rémy-Ruyer, A., Madden, S. C., Galliano, F., et al. 2014, A&A, 563, A31
                                                                                   Reuter, C., Spilker, J. S., Vieira, J. D., et al. 2023, ApJ, 948, 44
                                                                                   Reuter, C., Vieira, J. D., Spilker, J. S., et al. 2020, ApJ, 902, 78
                                                                                   Rigby, J., Perrin, M., McElwain, M., et al. 2023a, PASP, 135, 048001
                                                                                   Rigby, J. R., Lightsey, P. A., García Marín, M., et al. 2023b, PASP, 135,
                                                                                   Rupke, D. S. N., Kewley, L. J., & Chien, L. H. 2010, ApJ, 723, 1255
                                                                                   Rupke, D. S. N., Veilleux, S., & Baker, A. J. 2008, ApJ, 674, 172
                                                                                   Rybak, M., Hodge, J. A., Greve, T. R., et al. 2022, A&A, 667, A70
                                                                                   SandersR. L., Shapley, A. E., Clarke, L., et al. 2023, ApJ, 943, 75
                                                                                   SandersR. L., Shapley A. E., Kriek, M., et al. 2015, ApJ, 799, 138
                                                                                   Sanders, R. L., Shapley, A. E., Reddy, N. A., et al. 2020, MNRAS, 491, 1427
                                                                                   Spilker, J. S., Aravena, M., Marrone, D. P., et al. 2015, ApJ, 811, 124
                                                                                   Spilker, J. S., Marrone, D. P., Aguirre, J. E., et al. 2014, ApJ, 785, 149
                                                                                   Spilker, J. S., Marrone, D. P., Aravena, M., et al. 2016, ApJ, 826, 112
                                                                                   Spilker, J. S., Phadke, K. A., Aravena, M., et al. 2023, Natur, 618, 708
                                                                                   Steidel, C. C., Rudie, G. C., Strom, A. L., et al. 2014, ApJ, 795, 165
                                                                                   Strandet,M. L., Weiss,A., De Breuck,C., et al. 2017, ApJL, 842, L15
                                                                                   Sun, F., Egami, E., Fujimoto, S., et al. 2022, ApJ, 932, 77
                                                                                   Swinbank, A. M., Chapman, S. C., Smail, I., et al. 2006, MNRAS, 371, 465
                                                                                   Swinbank, A. M., Simpson, J. M., Smail, I., et al. 2014, MNRAS, 438, 1267
                                                                                   Tremonti, C. A., Heckman, T. M., Kauffmann, G., et al. 2004, ApJ, 613, 898
                                                                                  Troncoso, P., Maiolino, R., Sommariva, V., et al. 2014, A&A, 563, A58
                                                                                   Trump, J. R., Arrabal Haro, P., Simons, R. C., et al. 2023, ApJ, 945, 35
                                                                                   Vale Asari, N., Couto, G. S., Cid Fernandes, R., et al. 2019, MNRAS,
                                                                                      489,4721
                                                                                   Vieira, J. D., Marrone, D. P., Chapman, S. C., et al. 2013, Natur, 495, 344
                                                                                   Wisnioski, E., Förster Schreiber, N. M., Wuyts, S., et al. 2015, ApJ, 799, 209
                                                                                   Wuyts, E., Kurk, J., Förster Schreiber, M., et al. 2014, ApJL, 789, L40
Hayward, C. C., Sparre, M., Chapman, S. C., et al. 2021, MNRAS, 502, 2922 Zavala, J. A., Casey, C. M., Manning, S. M., et al. 2021, ApJ, 909, 165
```

Hopkins, P. F., Hernquist, L., Cox, T. J., & Kereš, D. 2008, ApJS, 175, 356